

Modeling of Interaction of Ions

with Ether- and Ester-linked phospholipids

by

Matthew W. Saunders

A thesis submitted in partial fulfillment  
of the requirements of the degree of  
Master of Science in Biology

with a concentration in Cell & Molecular Biology  
Department of Cell Biology, Microbiology and Molecular Biology  
College of Arts and Sciences  
University of South Florida

Major Professor: Sameer Varma, Ph.D.

Sagar Pandit, Ph.D.

H. Lee Woodcock, Ph.D.

Jianjun Pan, Ph.D.

# CONTENTS

<b>List of Tables</b>	<b>ii</b>
<b>List of Figures</b>	<b>iii</b>
<b>Abstract</b>	<b>iv</b>
<b>1 Introduction</b>	<b>1</b>
1.1 Ether- and Ester-linked Phospholipids . . . . .	1
1.2 Using Molecular Dynamics to Study Biological Membranes . . . . .	4
<b>2 Interaction of salt with ether- and ester-linked phospholipid bilayers</b>	<b>8</b>
2.1 Methods . . . . .	8
2.1.1 HOPC bilayer construction . . . . .	9
2.1.2 Simulation Details . . . . .	9
2.2 Results and Discussion . . . . .	10
2.2.1 Bilayer Structure . . . . .	10
2.2.2 Membrane-salt interactions . . . . .	15
2.2.3 Water structure and dynamics . . . . .	18
2.2.4 Bilayer electrostatics . . . . .	26
2.2.5 Salt distribution at the bilayer-solvent interface . . . . .	28
<b>3 Conclusions</b>	<b>33</b>



## LIST OF TABLES

## LIST OF FIGURES

1.1	Image of a model bilayer of phospholipids from a simulation. . . . .	2
1.2	Chemical structures of representative phospholipids highlighting the difference between ether- and ester-links. . . . .	3
2.1	Comparison of component mass densities between the HOPC and POPC systems. . . . .	11
2.2	Electron Densities of Simulated Systems. . . . .	14
2.3	Order parameters of lipid chains. . . . .	16
2.4	Comparison of headgroup component and ion number densities between the HOPC and POPC systems. . . . .	17
2.5	First shell coordination environment of $\text{Na}^+$ ions. . . . .	19
2.6	Cumulative radial distribution functions of water hydrogens around various lipid oxygens. . . . .	21
2.7	The first and second order parameters, $P_1$ and $P_2$ , of water O-H bonds. . . .	22
2.8	Orientational autocorrelation times of O-H bonds in water, as determined by modeling their autocorrelations using three-exponential fits. . . . .	25
2.9	Comparison of electrostatic potentials between the HOPC and POPC systems. .	27
2.10	Illustration of bulk ion distribution, with surfaces used in Gouy-Chapman theory calculations. . . . .	31
2.11	Comparison of Gouy-Chapman theory predictions and simulation results. . .	32

## ABSTRACT

Polar lipids, or phospholipids, are present in all parts of cells and are used in many signalling and structural roles. As structural molecules they act as the main component of cellular plasma membranes — bilayers of polar lipids that separate cells from their environments. Bilayer properties are heavily influenced by the structure of their component polar lipids, and different lipids are found in different organisms. A distinguishing feature of Archaeal plasma membranes is that their phospholipids contain ether-links, as opposed to bacterial and eukaryotic plasma membranes where phospholipids primarily contain ester-links. In our work we examine the effects of salt on bilayer structure in the case of an ether-linked lipid bilayer. We use molecular dynamics simulations and compare equilibrium properties of two model lipid bilayers in NaCl salt solution — POPC and its ether-linked analog that we refer to as HOPC. We make the following key observations. The headgroup region of HOPC “adsorbs” fewer ions compared to the headgroup region of POPC. Consistent with this, we note that the Debye screening length in the HOPC system is  $\sim 10\%$  shorter than that in the POPC system. Herein, we introduce a protocol to identify the lipid-water interfacial boundary that reproduces the bulk salt distribution consistent with Gouy-Chapman theory. We also note that the HOPC bilayer has excess solvent in the headgroup region when compared to POPC, coinciding with a trough in the electrostatic potential. Waters in this region have longer autocorrelation times and smaller lateral diffusion rates compared to the corresponding region in the POPC bilayer, suggesting that the waters in HOPC are more strongly coordinated to the lipid headgroups. Furthermore, we note that it is this region of tightly coordinated waters in the HOPC system that has a lower density of  $\text{Na}^+$

ions. Based on these observations we conclude that an ether-linked lipid bilayer has a lower binding affinity for  $\text{Na}^+$  compared to an ester-linked lipid bilayer.

# CHAPTER 1

## INTRODUCTION

### **1.1 Ether- and Ester-linked Phospholipids**

Phospholipids are a diverse species of biological molecules used in many roles in life.<sup>1</sup> These molecules are amphipathic, with a headgroup that is hydrophilic attached to hydrophobic acyl chains by a glycerol backbone.<sup>2,3</sup> These molecules, when above a critical concentration in aqueous solution, self assemble into various aggregate structures in order to reduce the exposure of the hydrophobic chains to polar solvent — these structures include micelles, vesicles, and bilayers along with others.<sup>3</sup> Phospholipids tend to form bilayers, where the hydrophilic headgroups face the solvent and the hydrophobic acyl chains face into the center of the structure.<sup>3,4</sup> An image of a bilayer of a commonly studied model lipid can be seen in figure 1.1. In living cells, lipid bilayers act as the delimiter between the cell and the environment, acting as one of the major constituents of the cellular plasma membrane.<sup>6</sup> The plasma membrane consists of a mixture of many lipid species, as well as proteins and lipid-like molecules, and the mixture is tuned by the cell to adapt the structure and flexibility of the plasma membrane to different environments.<sup>1,2,7</sup> Furthermore, the cellular membrane is the interface for exchange of nutrients with the environment, and also the interface for the transmission of signals to and from the outside of the cell. This exchange is done through passive diffusion, proteins and other molecules embedded into the membrane, and through the formation of vesicles and buds out of the lipid bilayer.<sup>6</sup> The behavior and function of

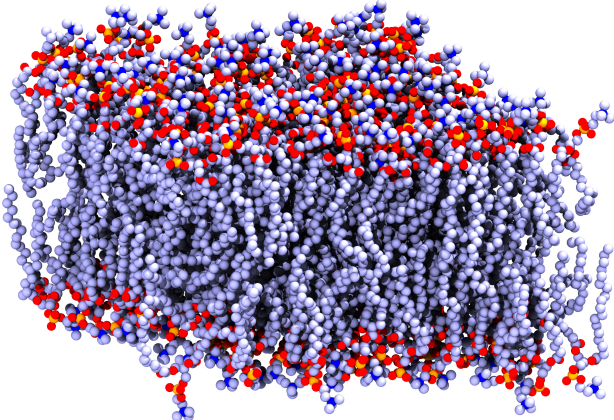


Figure 1.1: Image of a model bilayer of phospholipids from a simulation. The lipids can be seen in the center of the image, with the hydrophobic chains colored in light purple. The polar headgroup can be seen highlighted by the phosphate group in orange and the choline nitrogen in blue facing the solvent. Solvent molecules have been removed for clarity. Figure generated using VMD<sup>5</sup>

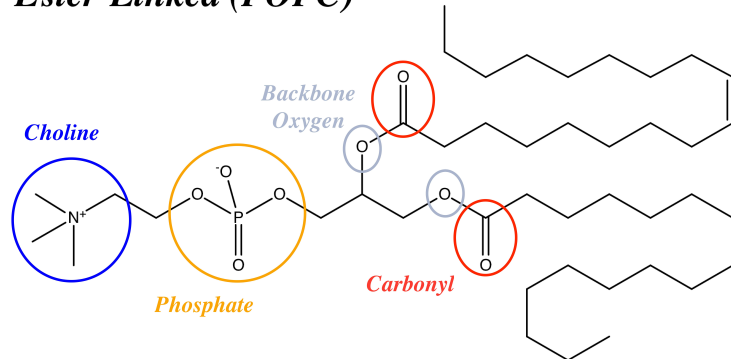
19 the plasma membrane is heavily dependent on the structure of the bilayer, which again can  
20 be influenced directly by the mixture of phospholipids constituting the membrane.<sup>1,7</sup>

21 Phospholipids can be modified in a variety of ways to change their chemical construction,  
22 and the structure of the individual molecules manifest significant changes in the stucture  
23 of aggregates, like lipid bilayers or cell membranes. Polar headgroups can be charged or  
24 zwitterionic.<sup>3</sup> The fatty acid chains can be saturated or unsaturated, and can have many  
25 lengths depending on the needs of the cell — differing the acyl chains influences the phase  
26 behavior of the bilayer, which can help cells to adapt to changes in temperature.<sup>4,7</sup>

27 Phospholipids can also use several types of chemical links between the glycerol back-  
28 bone and the fatty acid chains.<sup>8,9</sup> Phospholipids containing ether-links represent one of the  
29 many major evolutionary divides – while they make up much of the phospholipids of archaeal  
30 membranes, they are present in only small fractions in eukarya and bacteria.<sup>8–10</sup> These phos-  
31 pholipids differ from the more common ester-linked phospholipids of bacterial and eukaryotic  
32 membranes in that they lack fatty acid carbonyl groups (see figure 1.2).

33 The chemical difference between ester- and ether-linked lipids has been shown to influence  
34 bilayer properties including both structure and permeability.<sup>11–16</sup> Experiments show that

### **Ester-Linked (POPC)**



### **Ether-Linked (HOPC)**

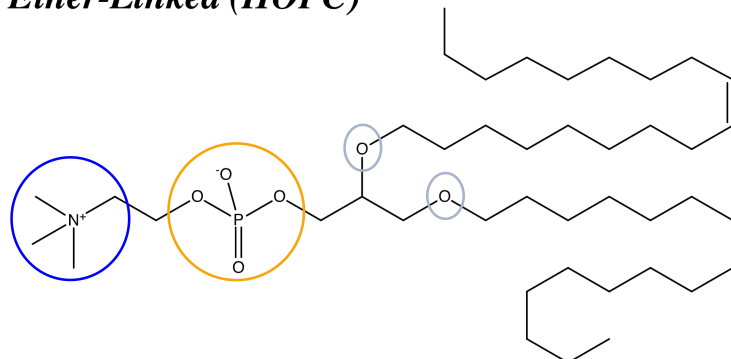


Figure 1.2: Chemical structures of representative phospholipids highlighting the difference between ether- and ester-links. POPC (1-palmitoyl-2-oleoyl-sn-glycero-3-phosphatidylcholine) is a diester lipid and HOPC (1-hexadecyl-2-(9-octadecenyl)-sn-glycero-3-phosphatidylcholine) is its diether analog that lacks fatty acid carbonyl groups.

35 model bilayers composed exclusively of ether-linked lipids have smaller dipole potentials  
36 compared to bilayers composed of their ester-linked analogs;<sup>13</sup> a result also predicted by  
37 a molecular dynamics (MD) study done by our group.<sup>16</sup> The interfacial water in ether-  
38 linked lipid bilayers is also more structured compared to that in ester-linked lipid bilayers,  
39 as observed in NMR experiments in the form a larger quadrupolar splitting constants,<sup>13</sup> and  
40 as also reproduced in our simulations.<sup>16</sup> Two independent experimental studies also show  
41 that ether-linked lipid bilayers are less permeable to water compared to bilayers composed  
42 of their ester-linked analogs.<sup>11,12</sup>

43 Nevertheless, all studies aimed at examining differences between ester- and ether-linked  
44 lipid bilayers have been carried out in pure water, except for the one recent study by Leonard  
45 *et al.*<sup>17</sup> As such, several studies show that salt significantly affects the properties of ester-  
46 linked lipid bilayers.<sup>18–23</sup> For example, in our previous works on the interactions of monova-  
47 lent and divalent ions on zwitterionic ester-linked lipid bilayers<sup>18,19</sup> we found that monovalent  
48 cations insert into headgroup region. We reported reduction in area per lipid, increase in  
49 bilayer thickness, increased range of ordered solvent at the bilayer surface, and an increase in  
50 the electrostatic dipole potential of the bilayer. Despite the work done on these lipids in the  
51 past, the question of how ions interact with bilayers of ether-linked phospholipids compared  
52 to ester-linked remains a topic of interest.

## 53 1.2 Using Molecular Dynamics to Study Biological Mem- 54 branes

55 In order to explore the question of how ions interact with bilayers of ether- and ester-  
56 linked lipids, we utilize Molecular Dynamics (MD) simulations.

57 Computational methods like molecular dynamics must strike a balance between compu-  
58 tational cost and accuracy. The most expensive computations using *ab initio* methods with  
59 minimal approximations are the most accurate, but are only feasible for very small systems.<sup>24</sup>  
60 For biologically relevant systems, a classical approximation is able to reproduce most impor-

tant phenomena.<sup>2,24</sup> MD makes this classical approximation, expressing particles as points in space, with masses centered at the nucleus.<sup>2</sup> Functional forms and functional parameters needed to calculate the hamiltonian of systems are defined in a force-field. Bonds and bond angles are modeled as harmonic potentials, and torsional parameters within molecules are modeled using periodic functions. Non-bonded interactions are modeled using simple pairwise-additive potentials and generally do not treat many-body interactions.<sup>2,25</sup> Van der Waals (VdW) dispersion and hard-shell repulsion are usually treated using a Lennard-Jones 6-12 potential, and short-range electrostatics are represented by a coulomb potential.<sup>2,25</sup> The potential terms are added together over the whole system of particles to get the overall potential function of the system, which is then used to evolve the system over time by integrating Newton's laws of motion.<sup>26</sup> An example of the total potential can be seen in equation 1.1.<sup>2</sup>

$$\begin{aligned}
 V_{tot} = & \sum_{\text{bonds}} K_b(r - r_0)^2 \\
 & + \sum_{\text{angles}} K_\theta(\theta - \theta_0)^2 \\
 & + \sum_{\text{improper}} K_\Phi(\Phi - \Phi_0)^2 \\
 & + \sum_{\text{torsion}} K_\phi[1 - \cos(n\phi - \phi_0)] \\
 & + \sum_{\text{Estatic}} \frac{q_i q_j}{r_{ij}} \\
 & + \sum_{VdW} \frac{A_{ij}}{r_{ij}^{12}} - \frac{B_{ij}}{r_{ij}^6}
 \end{aligned} \tag{1.1}$$

Most force-fields for molecular dynamics treat charges on particles in the system as an average picture of overall electronic behavior, as the timescale of electronic fluctuations is much smaller than the timescale of MD simulations; this means bonds are permanent, and average charge densities are fixed to particles.<sup>2</sup> Some force fields treat electronic polarizability as an explicit term in the potential function;<sup>27,28</sup> however most MD force-fields do not include this while still giving a good reproduction of experimental results.<sup>2,17,32</sup>

79 To ensure accurate reproduction of experimental results from complex systems, force-  
80 fields are developed and optimized to directly reproduce experimental data in simple model  
81 systems. To develop force-fields, systems of small molecules can be optimized to repro-  
82 duce experimental heats and enthalpies of vaporization, molecular volumes, and densities of  
83 condensed phases.<sup>29–32</sup> For systems of whole lipid bilayers, experimental methods such as  
84 deuterium NMR, small angle x-ray scattering, and small angle neutron scattering can be  
85 used to get ensemble average values for bilayer ordering and structure and are often used to  
86 validate lipid simulations.<sup>2,15–17,19,27,32,33</sup> We can also look at electrostatic properties such  
87 as the bilayer electrostatic dipole potentials,<sup>13,34</sup> or mechanical properties like bilayer com-  
88 pressibility or surface tension.<sup>16,19,35</sup> For optimization of force-fields using small molecules,  
89 experimental heats and enthalpies of vaporization, molecular volumes, and densities of con-  
90 densed phases can be used.<sup>29–32</sup>

91 The earliest lipid simulations often used a united atom representation of the lipids, which  
92 simplified lipid chains by expressing carbon groups as beads rather than explicitly defining  
93 hydrogens.<sup>36–38</sup> These simulations focused on validation with experimental values for bilayer  
94 structure, such as area per lipid and bilayer thickness that are taken from SAXS and SANS  
95 measurements. Later development of force-fields included calculating partial charges for  
96 different parts of the lipid molecules using *ab initio* quantum calculations.<sup>37,39</sup> Chiu *et*  
97 *al.* calculated charges in this way for the GROMOS force-field of DPPC in 1995.<sup>39</sup>

98 Berger *et al.* sought to further improve the densities given by the GROMOS force-field in  
99 1997 by optimizing VdW parameters using molecular volumes and heats of vaporization in  
100 small hydrocarbon molecules to improve the acyl chains of DPPC,<sup>29</sup> work that was contin-  
101 ued by Chiu *et al.*,<sup>30,31</sup> Later, further optimization was carried out by Chiu *et al.* in 2009 to  
102 improve torsional and VdW parameters using experimental heats of vaporization and den-  
103 sities, and validated the overall result by predicting small-angle x-ray scattering results for  
104 model lipid bilayers to create the GROMOS 43-A1S3 lipid force field which gave excellent  
105 reproduction of SAXS form-factors for different lipids.<sup>32</sup>

<sup>106</sup> Molecular dynamics can give this resolution while still reproducing the large-scale prop-  
<sup>107</sup> erties of the system as a whole.<sup>2,24</sup> Properties of the lipid bilayer can be expressed directly  
<sup>108</sup> in terms of the positions or dynamics of atoms, providing additional understanding of these  
<sup>109</sup> systems.

110

## CHAPTER 2

111

### INTERACTION OF SALT WITH ETHER- AND ESTER-LINKED PHOSPHOLIPID BILAYERS

113

In this work we seek to answer the general questions of how salt interacts with ether-linked lipid bilayers, and how ether-linked lipid bilayers differ from ester-linked lipid bilayers in the presence of salt. We addressed these questions by carrying out a molecular dynamics simulation of 1-hexadecyl-2-(9-octadecenyl)-sn-glycero-3-phosphatidylcholine lipid bilayer (HOPC) in NaCl salt. We also compared results of this simulation against our previous simulation of 1-palmitoyl-2-oleoyl-sn-glycero-3-phosphatidylcholine lipid bilayer (POPC) in NaCl.<sup>19</sup> Additionally, to gain insight into how salt modulates differences between ether- and ester-linked lipid bilayers, we also compared these simulations against those of ether- and ester-linked lipid bilayers in pure water.<sup>16</sup>

122

### 2.1 Methods

123

The trajectories for the POPC bilayer in 200 mM NaCl were taken from our previous work,<sup>19</sup> and were re-analyzed to address the specific goals of this project. The trajectories for the HOPC bilayer were generated as described below, following the same protocol we used for the POPC bilayer. Analysis was carried out using GROMACS<sup>40-44</sup> utility tools, and in-house software developed using GROMACS API.

<sup>128</sup> **2.1.1 HOPC bilayer construction**

<sup>129</sup> To construct the HOPC bilayer, we first place 100 lipids on  $10 \times 10$  nm grid to form  
<sup>130</sup> a bilayer leaflet, and then reflect the leaflet to create the second leaflet of the bilayer. We  
<sup>131</sup> then introduce 30,000 water molecules into the space outside the bilayer, which gives a 150:1  
<sup>132</sup> waters to lipid ratio. We then replace 216 randomly-selected waters with 108  $\text{Na}^+$  and 108  
<sup>133</sup>  $\text{Cl}^-$  ions to set an initial NaCl concentration of 200 mM. Note that the high water to lipid  
<sup>134</sup> ratio is necessary to get a good representation of bulk solvent, as the addition of salt increases  
<sup>135</sup> the distance of solvent ordering from the bilayer surface.<sup>19</sup> We then remove bad contacts  
<sup>136</sup> by energy minimizing using the steepest descent approach. Finally, we subject the system  
<sup>137</sup> to one cycle of annealing. Heating is done under constant pressure to 500K, but in steps  
<sup>138</sup> of 100K to avoid excess kinetic energy divergence. During heating, each step is simulated  
<sup>139</sup> for 10 ps. Cooling is also performed under constant pressure, but in smaller decrements –  
<sup>140</sup> cooling from 500K to 400K is done in 5 steps, and cooling from 400K to 300K in steps of 10  
<sup>141</sup> steps. Each cooling step is simulated for 50 ps. The total annealing time is 850 ps.

<sup>142</sup> **2.1.2 Simulation Details**

<sup>143</sup> MD simulation is performed using GROMACS version 5.1.5.<sup>40–44</sup> Water is described using  
<sup>144</sup> the SPC/E model,<sup>45</sup> and we use the united atom Gromos 43A1-S3 parameters for lipids and  
<sup>145</sup> lipid-water cross terms developed by our group.<sup>16,32</sup> These parameters have been verified in  
<sup>146</sup> previous works without salt against experimental SAXS data to ensure accurate reproduction  
<sup>147</sup> of bilayer structure.<sup>16</sup> Parameters for HOPC are derived from those for ether-linkages used for  
<sup>148</sup> di-hexadecyl phosphatidylcholine developed for previous work without ions.<sup>16</sup> Ion-ion and  
<sup>149</sup> ion-water interactions are described using parameters developed by Joung and Cheatham  
<sup>150</sup> III,<sup>46</sup> and the ion-lipid cross terms are calculated explicitly using Lorentz–Berthelot rules.<sup>19</sup>  
<sup>151</sup> These ion parameters were verified in previous work for binding constants as well as electro-  
<sup>152</sup> static potential, and we reported good reproduction of experimental results.<sup>19</sup> Temperature

<sup>153</sup> is held constant at 300K using the Nosé-Hoover thermostat,<sup>47</sup> and a coupling constant of 0.5  
<sup>154</sup> ps. Pressure is maintained at 1 bar using the Parrinello-Rahman semisotropic barostat,<sup>48</sup>  
<sup>155</sup> and a pressure coupling constant of 1.5 ps. All bonds are constrained using the P-LINCS  
<sup>156</sup> algorithm.<sup>49</sup> Neighbor-lists are updated every other time step, and integration is carried out  
<sup>157</sup> using the leap-frog Verlet scheme. Long-range electrostatics beyond 16 Å are computed using  
<sup>158</sup> the smooth particle mesh Ewald algorithm,<sup>50</sup> and Lennard-Jones interactions are calculated  
<sup>159</sup> with a cutoff of 16 Å. As before,<sup>19</sup> a continuous MD simulation is run for 0.5 μs.

## <sup>160</sup> 2.2 Results and Discussion

### <sup>161</sup> 2.2.1 Bilayer Structure

<sup>162</sup> We first compare mass densities of the different chemical components of HOPC against  
<sup>163</sup> those of POPC (see figure 2.1).

<sup>164</sup> We find that the headgroup region of HOPC has a higher density of solvent compared  
<sup>165</sup> to POPC – this is visible as a distinct peak in the solvent density profile in the HOPC  
<sup>166</sup> system. We verified that this additional peak does not result from accumulation of ions by  
<sup>167</sup> comparing mass density profiles of only water molecules. This peak is similar to observations  
<sup>168</sup> of a smaller peak made in our previous simulations in the absence of salt, and may be a direct  
<sup>169</sup> result of the ether-linked lipids.<sup>16</sup>

<sup>170</sup> Table 2.1 compares the structural properties of HOPC and POPC bilayers. Lipid volumes  
<sup>171</sup>  $V_l = V_c + V_{hg}$ , where  $V_c$  and  $V_{hg}$  are the volumes of lipid chains (tails) and headgroups.  
<sup>172</sup> These are computed using the approach given in Petrache et al.<sup>51</sup> In this approach, we first  
<sup>173</sup> compute the number densities  $n_i(z)$  of the various system components as a function of the  
<sup>174</sup> bilayer normal ( $z$ ). We then use these  $n_i(z)$  to determine their partial molecular volumes,  
<sup>175</sup>  $v_i$ , by optimizing the objective function,

$$\Omega(v_i) = \sum_{z_j}^{n_s} \left(1 - \sum_{i=1}^{N_{\text{groups}}} (n_i(z_j)v_i)\right)^2. \quad (2.1)$$

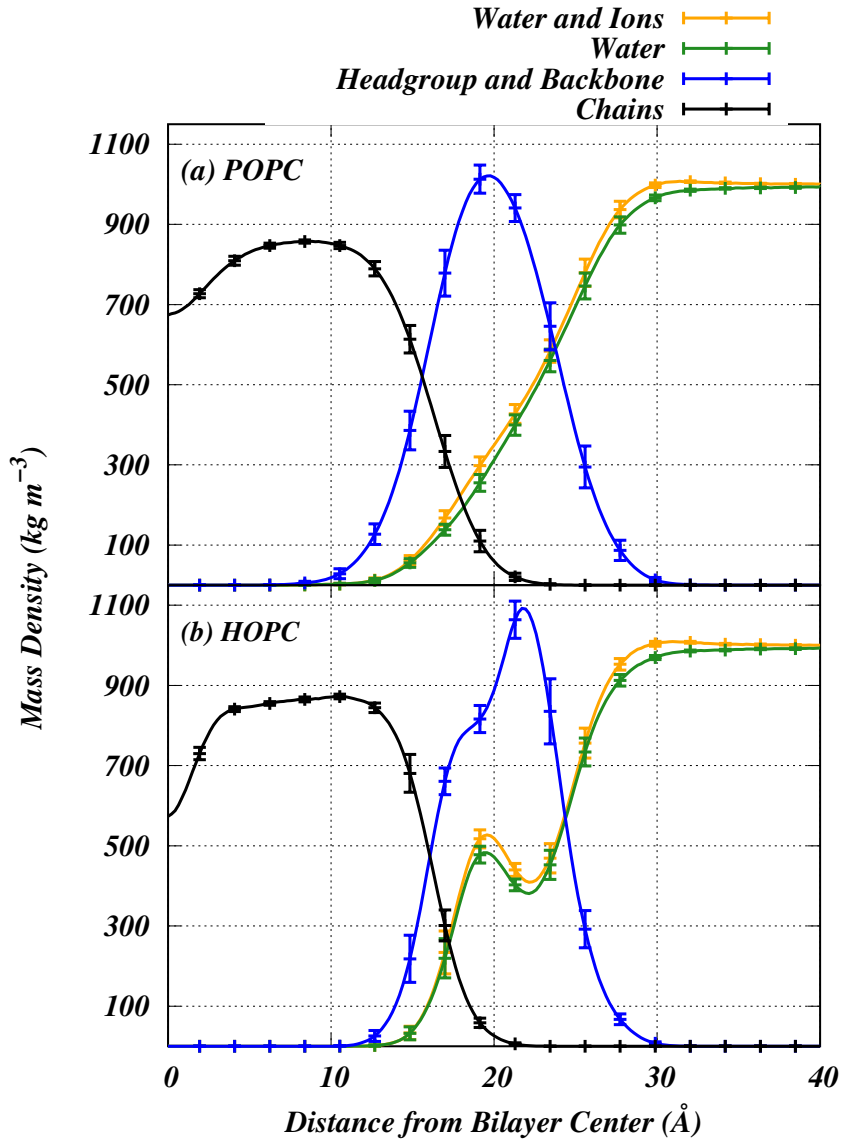


Figure 2.1: Comparison of component mass densities between the HOPC and POPC systems. Densities are computed by dividing the box dimension along the membrane normal into 2000 slices. For clarity of presentation, error bars are indicated for every 10th slice. Mass densities of solvent and ions, water, lipid headgroup and backbone, and lipid chains are shown. The plot for HOPC shows a peak in the water density inside the headgroup region that is not present in POPC, similar to what was seen in our previous work with DHPC.<sup>16</sup>

	POPC with NaCl	HOPC with NaCl
$V_c$ ( $\text{\AA}^3$ )	$898.4 \pm 1.2$	$900.0 \pm 1.0$
$V_h$ ( $\text{\AA}^3$ )	$318.9 \pm 0.9$	$290.2 \pm 0.9$
$V_l$ ( $\text{\AA}^3$ )	$1217.3 \pm 0.5$	$1190.2 \pm 0.9$
$2D_c$ ( $\text{\AA}$ )	$30.95 \pm 0.32$	$32.13 \pm 0.25$
$D_b$ ( $\text{\AA}$ )	$46.22 \pm 0.49$	$46.05 \pm 0.34$
$A_l$ ( $\text{\AA}^2$ )	$58.07 \pm 0.63$	$56.03 \pm 0.45$
$D_{hh}$ ( $\text{\AA}$ )	$40.24 \pm 0.75$	$42.62 \pm 0.88$
$N_w$	22.6	22.3
$\Delta\nu$ (Hz)	194.99	1756.08

Table 2.1: Comparison of HOPC and POPC bilayer structure properties:  $V_l$  is the lipid volume;  $V_c$  and  $V_h$  are the partial volumes of lipids chains and headgroups, respectively;  $2D_c$  and  $D_b$  are chain and bilayer thickness, respectively;  $A_l = V_c/D_c$  is the area per lipid.  $N_w$  is the number of perturbed waters in the system, defined as those behind the *hydration boundary*.  $\Delta\nu$  is the quadrupolar splitting constant of each system.

176 Here,  $N_{\text{groups}} = 7$  are the different system components including methyls ( $v_{CH_3}$ ), methines  
177 ( $v_{CH_2}$ ), methylenes ( $v_{CH}$ ), headgroup carbons, headgroup and backbone oxygens, headgroup  
178 phosphate and nitrogen, and water ( $v_{H_2O}$ ). Using these partial molecular volumes, we com-  
179 pute  $V_c = 2v_{CH_3} + 2v_{CH_1} + 28v_{CH_2}$  and  $V_{hg} = 10v_{hg_C} + 2v_{P\&N} + 8v_{hg_O}$ . We find that the  
180 headgroup volume of HOPC is 27.1 Å<sup>3</sup> smaller than POPC, due likely to the absence of car-  
181 bonyl groups. As expected for lipids with the same hydrocarbon chains, the chain volumes  
182 are similar in the two lipids.

183 We also use the number densities computed above ( $n_i(z)$ ) to determine lipid chain  
184 thickness ( $2D_c$ ) and bilayer thickness ( $D_b$ ). These results are found experimentally from  
185 x-ray and neutron scattering.<sup>15</sup> In our simulations these parameters are found by first  
186 computing the probability of finding the  $i$ -th group in each slice of the simulation box,  
187  $P_i(z) = n_i(z)/\sum_i n_i(z)$ . We define  $2D_c$  as the distance between the Gibbs' surfaces on the  
188 interfacial probability densities of lipid chains. Each of the two surfaces is computed by  
189 identifying the point on the curve where the integrals of probability densities in the interfa-  
190 cial regions above and below the surface are equal. We compute  $D_b$  in a similarly, but from  
191 solvent probability densities. We find that both POPC and HOPC have similar membrane  
192 thicknesses ( $D_b$ ); however a comparison of  $2D_c$  indicates that the hydrophobic chains in  
193 HOPC are slightly thicker than those in POPC, reflecting tighter chain packing. This is also  
194 evident from comparison of electron densities (see figure 2.2).

195 Electron density distributions are experimentally measured using x-ray scattering, by  
196 taking the reverse-fourier transform of the scattering form-factor.<sup>2,15,33</sup> Since the experi-  
197 mental x-ray scattering is dependent on the model used to compute the reverse-transform,  
198 we often calculate the form-factor of our simulated bilayer to compare to experiment by  
199 transforming the electron density distribution.<sup>16,19,32</sup> Since such data is not available for our  
200 current lipid system as far as we know, we cannot do this comparison here.

201 We also use the electron density distribution to calculate the peak-to-peak distance  $D_{hh}$ ,  
202 which is used another measure of the bilayer thickness. This is roughly reflective of the

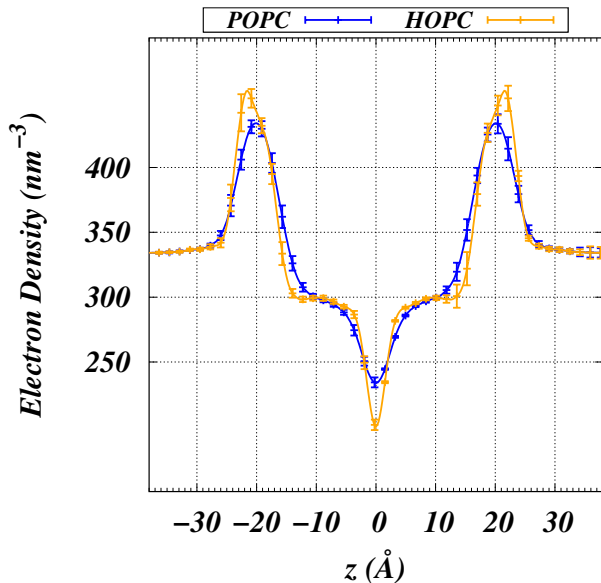


Figure 2.2: Electron Densities of Simulated Systems. Symmetrized electron density distribution of each simulated system as a function of  $z$ . We can see the distribution for HOPC is broader, with a longer peak-to-peak distance than in the POPC distribution. Furthermore, we see a deeper trough in the middle of the HOPC distribution. This plot was made by using the gromacs densities tool, dividing the system into 2000 slices. This data was calculated for every five nanoseconds, and averaged over the last 150ns of trajectories. Errorbars are shown for every 10th data point.

203 distance between the electron-dense phosphate groups on either bilayer leaflet.

204  $D_{hh}$  values for POPC and HOPC indicate that the ether-linked bilayer is  $\sim 2\text{\AA}$  thicker on  
205 average than the ester-linked bilayer. This discrepancy between the values of  $D_b$  and  $D_{hh}$  is  
206 likely due to the irregular shape of the distribution of solvent in the headgroup of HOPC —  
207 the extra region of solvent accumulation may move the Gibbs' surface used for finding  $D_b$   
208 into the bilayer surface.

209 The difference in bilayer thickness can also be shown directly from comparison of chain  
210 order parameters (See figure 2.3). As lipid chains become more ordered on average, bilayer  
211 thickness increases.<sup>33</sup>

212 We determine chain order parameters from the chain order tensor  $S_{\alpha\beta}$  defined as

$$S_{\alpha\beta} = \frac{1}{2} \left\langle 3 \cdot \cos(\theta_\alpha) \cdot \cos(\theta_\beta) - \delta_{\alpha\beta} \right\rangle, \quad (2.2)$$

213 where  $\theta_\alpha$  and  $\theta_\beta$  are the angles made by the molecular axes with  $\alpha$  and  $\beta$  as either  $x$ ,  $y$ , or  
214  $z$ , and  $\delta_{\alpha\beta}$  is the Kronecker-delta function. For the saturated bonds<sup>52</sup>

$$-S_{CD}^{Sat} = \frac{2}{3}S_{xx} + \frac{1}{3}S_{yy}, \quad (2.3)$$

215 and for unsaturated bonds<sup>53</sup>

$$-S_{CD}^{Unsat} = \frac{1}{4}S_{zz} + \frac{3}{4}S_{yy} \mp \frac{\sqrt{3}}{2}S_{yz} \quad (2.4)$$

216 We then use  $V_c$  and  $D_c$  to calculate areas per lipid,  $A_l = V_c/D_c$ . We find that the lateral  
217 surface area of HOPC is slightly smaller than that of the POPC bilayer.

## 218 2.2.2 Membrane-salt interactions

219 Ions prefer to associate or coordinate with specific sites in the headgroup regions of  
220 the lipid bilayers (See figure 2.4) —  $\text{Na}^+$  ions near phosphates and  $\text{Cl}^-$  ions near cholines.

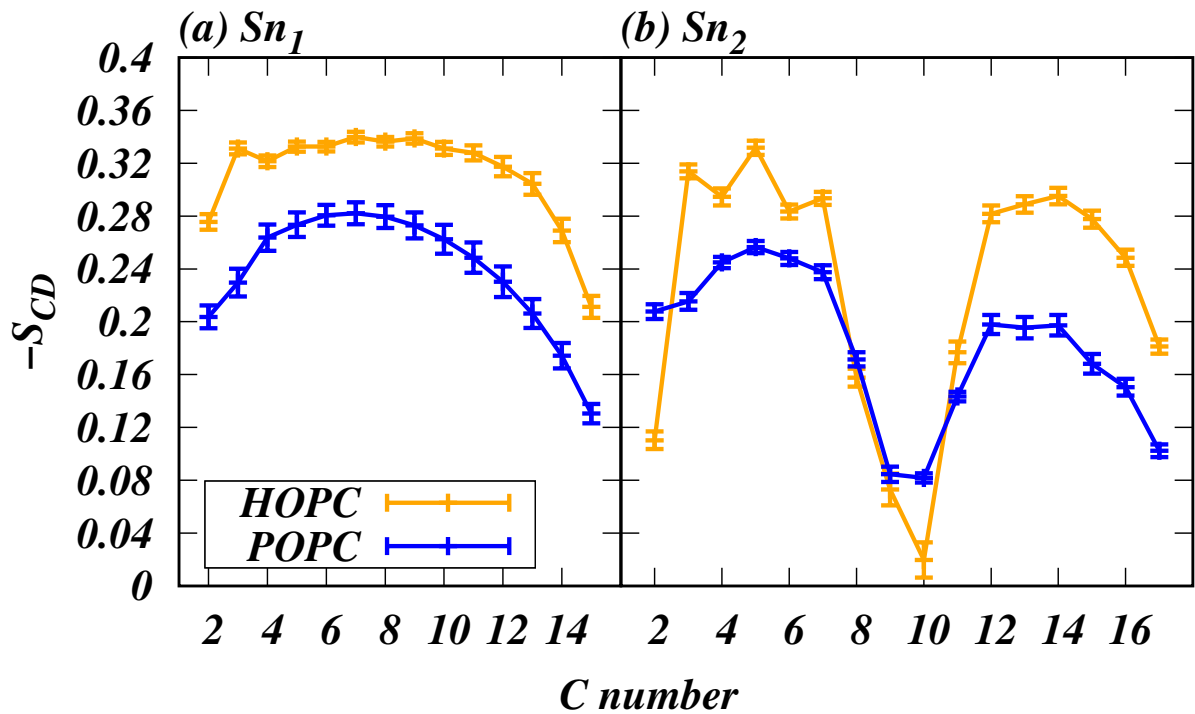


Figure 2.3: Order parameters of lipid chains.  $Sn_2$  and  $Sn_2$  refer to the two lipid tails. The carbon numbering starts from the polar carbon at the ester bond; however, we do not calculate an  $S_{CD}$  for the first carbon as this carbon would not have a hydrogen attached in an ester-linked lipid. This convention was maintained for the ether-linked lipid. The unsaturated bond is between carbons 9 and 10 on the  $Sn_2$  chain. In both chains, HOPC shows higher ordering, except for the unsaturated carbons on the 9-octadecene chain. This ordering corresponds with the lower area per lipid of the HOPC bilayer, values of which can be seen in table 2.1.

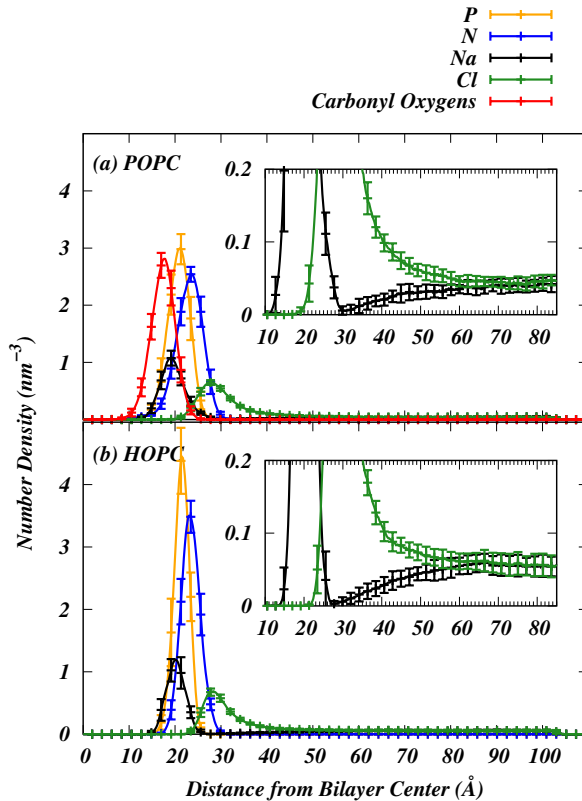


Figure 2.4: Comparison of headgroup component and ion number densities between the HOPC and POPC systems. The inset zooms in on the ordinate axis to visualize the extent of ion adsorption into bilayer as well as ion densities in the bulk. Densities are computed by dividing the box dimension along the membrane normal into 2000 slices. Error bars are indicated for every 10th slice. We note that sodium ions have a broader distribution in POPC than in HOPC. The peak of the  $\text{Na}^+$  distribution in POPC is also closer to the center of the bilayer than in HOPC. This may be due to the interaction of ions with the carbonyl oxygens (shown in red) that are present in POPC but absent in HOPC. In both bilayers, the chloride ions gather near the positively charged choline trimethylammonium, shown in blue. The inset shows the distribution of ions in the transitional region from the bilayer surface to bulk solvent. As one looks further out from the bilayer, the density of  $\text{Na}^+$  and  $\text{Cl}^-$  equalize, as is expected in bulk solvent.

<sup>221</sup> Here we note that ion peaks are positioned similarly in both HOPC and POPC systems.  
<sup>222</sup> Cl<sup>-</sup> ions do not enter the bilayer headgroup region, while Na<sup>+</sup> ions move far into this region  
<sup>223</sup> of the bilayer surface. However, the Na<sup>+</sup> densities trail off deeper into the POPC bilayer  
<sup>224</sup> by  $\sim 5 \text{ \AA}$  (visible in the inset of figure 2.4). In fact, we find that more ions localize in  
<sup>225</sup> the POPC bilayer — Averaged over the last 150 ns we see  $74.45 \pm 0.56$  Na<sup>+</sup> ions bound  
<sup>226</sup> to POPC, compared to  $62.27 \pm 2.00$  Na<sup>+</sup> ions bound to HOPC. We consider an ion to be  
<sup>227</sup> bound to the membrane when half or fewer of the inner-shell coordination partners of the  
<sup>228</sup> ion are waters. The inner shell of Na<sup>+</sup> ions is defined using a cutoff of  $3.15 \text{ \AA}$  based on radial  
<sup>229</sup> distribution functions of Na<sup>+</sup> with the water oxygens.<sup>54</sup> The Cl<sup>-</sup> ions do not lose waters and  
<sup>230</sup> do not seem to adsorb on the bilayer, hence we have not analyzed the binding behavior of  
<sup>231</sup> Cl<sup>-</sup> in this work. Figure 2.5 shows the inner-shell coordination environment of Na<sup>+</sup> ions as  
<sup>232</sup> a function of their positions in the bilayer. For this, we used a cutoff of  $3.3 \text{ \AA}$ , based on the  
<sup>233</sup> radial distribution functions of Na<sup>+</sup> with the various lipid oxygens (data not shown). When  
<sup>234</sup> Na<sup>+</sup> ions are bound, they are primarily coordinated by phosphate oxygens — this holds for  
<sup>235</sup> both HOPC and POPC. The main difference between POPC and HOPC is in how carbonyl  
<sup>236</sup> oxygens, backbone oxygens, and water oxygens coordinate with ions. In POPC, ions are  
<sup>237</sup> partially coordinated by both carbonyl oxygens and water, but not by backbone oxygens;  
<sup>238</sup> however, in HOPC backbone oxygens do partially coordinate Na<sup>+</sup>. This may contribute  
<sup>239</sup> to the deeper penetration of Na<sup>+</sup> into the POPC bilayer, and the greater number of ions  
<sup>240</sup> adsorbed onto the POPC bilayer surface when compared to HOPC.

### <sup>241</sup> 2.2.3 Water structure and dynamics

<sup>242</sup> As we noted above in Figure 2.1, the headgroup region of HOPC has a higher density of  
<sup>243</sup> water than POPC. We have also noted previously that in general salts tend to extend the  
<sup>244</sup> region of structured water near the bilayer surface.<sup>19</sup> To gain further insight into how the  
<sup>245</sup> absence of carbonyl groups in ether lipid bilayers increases water density, we systematically  
<sup>246</sup> characterize the structure and dynamics of water.

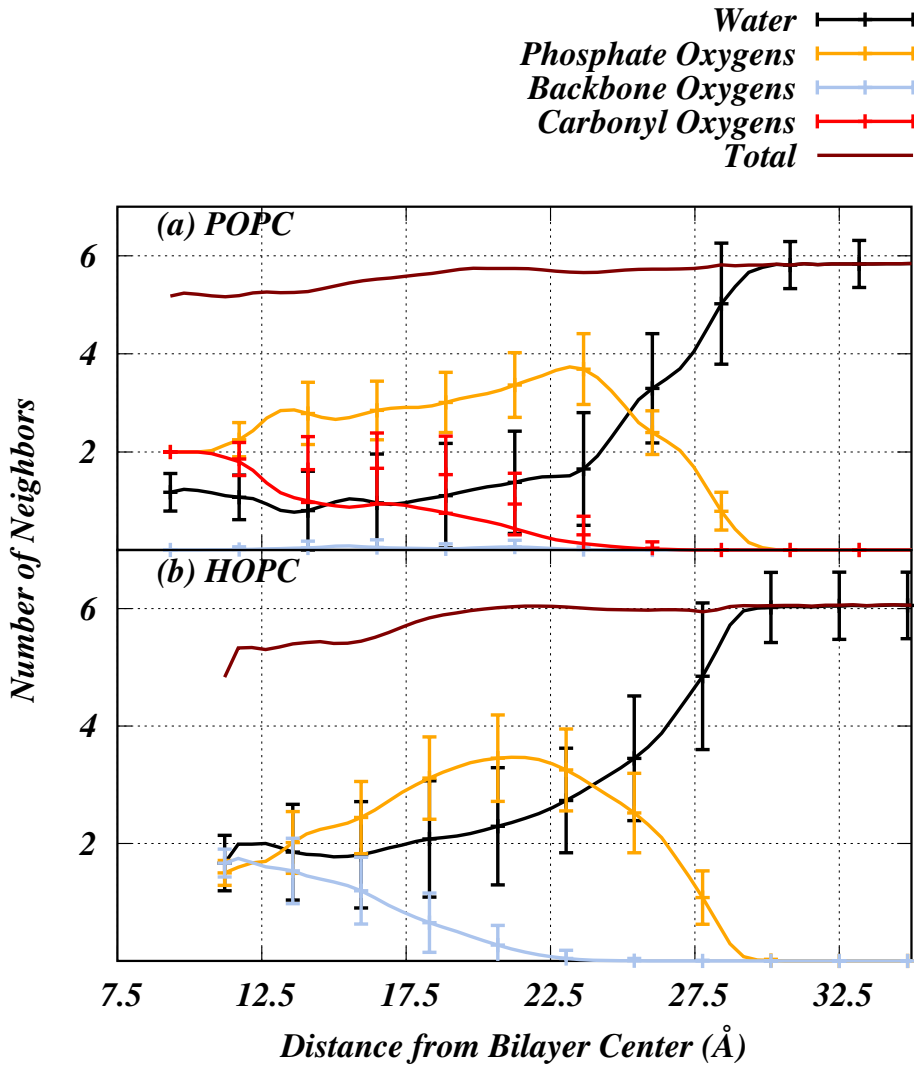


Figure 2.5: First shell coordination environment of  $\text{Na}^+$  ions. The cutoff distance for the first shell is taken as 3.3 ångströms, based on the radial distribution function of  $\text{Na}^+$  with the various lipid oxygens. This chart was made by dividing the box into 400 slices, and then symmetrizing around the bilayer center. Data is averaged over the last 100ns of simulation trajectory. Errorbars are shown for every tenth data point. Note that the coordination number of  $\text{Na}^+$  drops from 6 to 5 as it interacts deeper in both bilayers, and this drop occurs sooner in the HOPC system than in POPC. No values are shown for at distances less than 7.5 Å from the bilayer center, due to the lack of ions beyond in this region.

247      Figure 2.6 compares the integrated radial distribution of water hydrogens around lipid  
248      oxygens. We note that there is very little water directly coordinating the backbone oxygens  
249      in the POPC bilayer ( $\sim 1/3$  water per lipid). Compared to backbone oxygens, more water  
250      directly coordinates the ester carbonyl oxygens and the phosphate oxygens in POPC. We see  
251      a larger number of waters coordinating with the backbone oxygens in HOPC than in POPC,  
252      nearly 2 waters per lipid. Therefore, we attribute the higher density of water in HOPC to  
253      coordination with backbone oxygens.

254      Note that in POPC, carbonyls oxygens compete with phosphates for water coordination.  
255      Consequently, we expect waters to have a greater average ordering in the HOPC headgroup.  
256      We had observed this greater ordering in our previous comparative study of diether- and  
257      diester-lipid bilayers.<sup>16</sup>

258      In order to further explore solvent ordering by the bilayer surface, we compute order  
259      parameters of water O-H bonds. The first order parameter ( $P_1$ ) is calculated by time-  
260      averaging the cosine of the angle  $\theta$  that the OH bond makes with the bilayer normal, that  
261      is  $P_1 = \langle \cos(\theta) \rangle$ . Consequently, a positive value represents an orientation away the bilayer.  
262      The second parameter, which is defined as the second Legendre polynomial of  $\cos(\theta)$ , that  
263      is,  $P_2 = \langle (3 \cdot \cos^2(\theta) - 1) \rangle / 2$ . We calculate both  $P_1$  and  $P_2$  as a function of position along  
264      the bilayer normal, and they are shown in figure 2.7.

265      We find that the water in the headgroup region is clearly more ordered in the HOPC  
266      bilayer. Figure 2.7b shows the second order parameter. We note that the induced perturba-  
267      tions in the water layer are more prominent in HOPC than that of POPC. At the same time,  
268      however, we find that the numbers of water that are ordered in the two systems are similar.  
269      We count the average number of non-bulk (perturbed) waters as waters within the non-zero  
270      region of the second order parameter. We find this boundary by fitting an exponential func-  
271      tion to the region starting at the peak in the first order parameter, and taking the inverse  
272      of the length-scale of the fitted function as the position of the surface. The region beyond  
273      this point is considered bulk water. We will refer to this surface as the *hydration boundary*

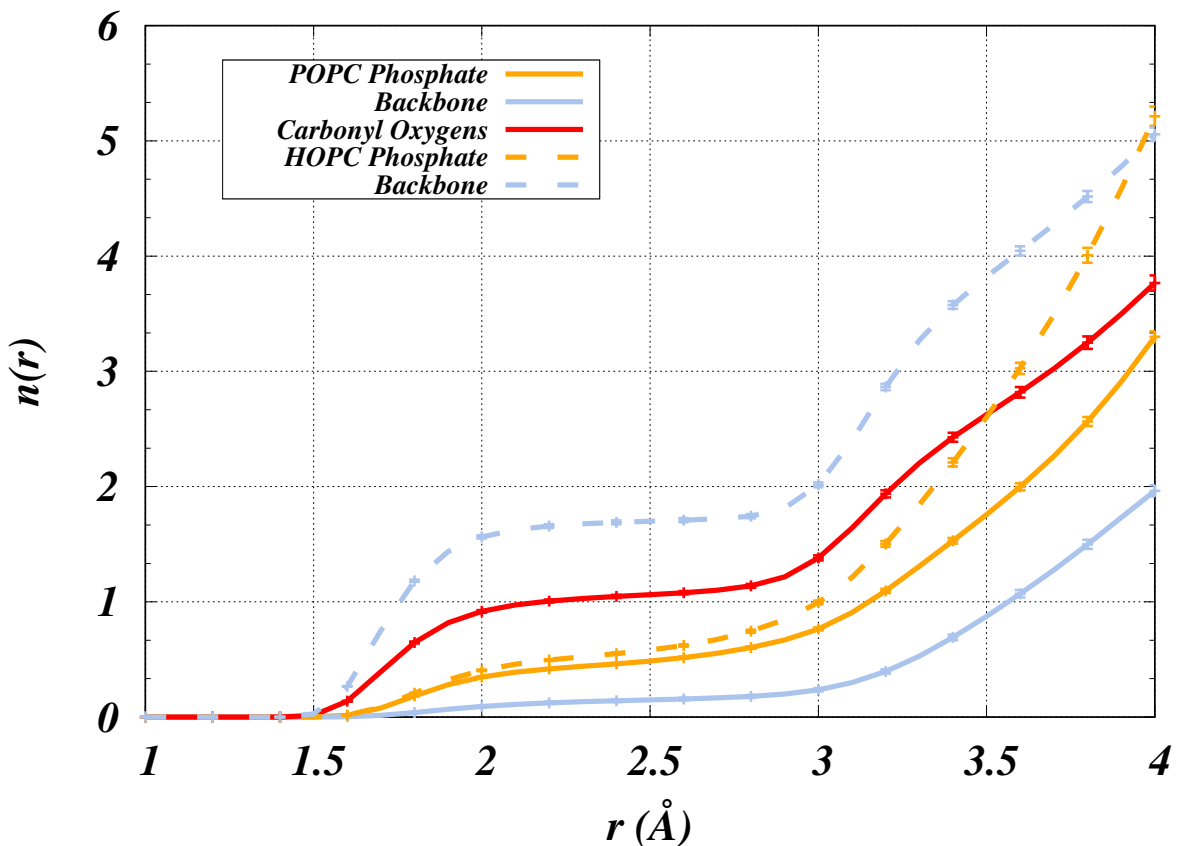


Figure 2.6: Cumulative radial distribution functions of water hydrogens around various lipid oxygens. The distributions for POPC are shown in solid lines, while HOPC is shown with dotted lines. The oxygens are grouped into categories as denoted in figure 1.2.

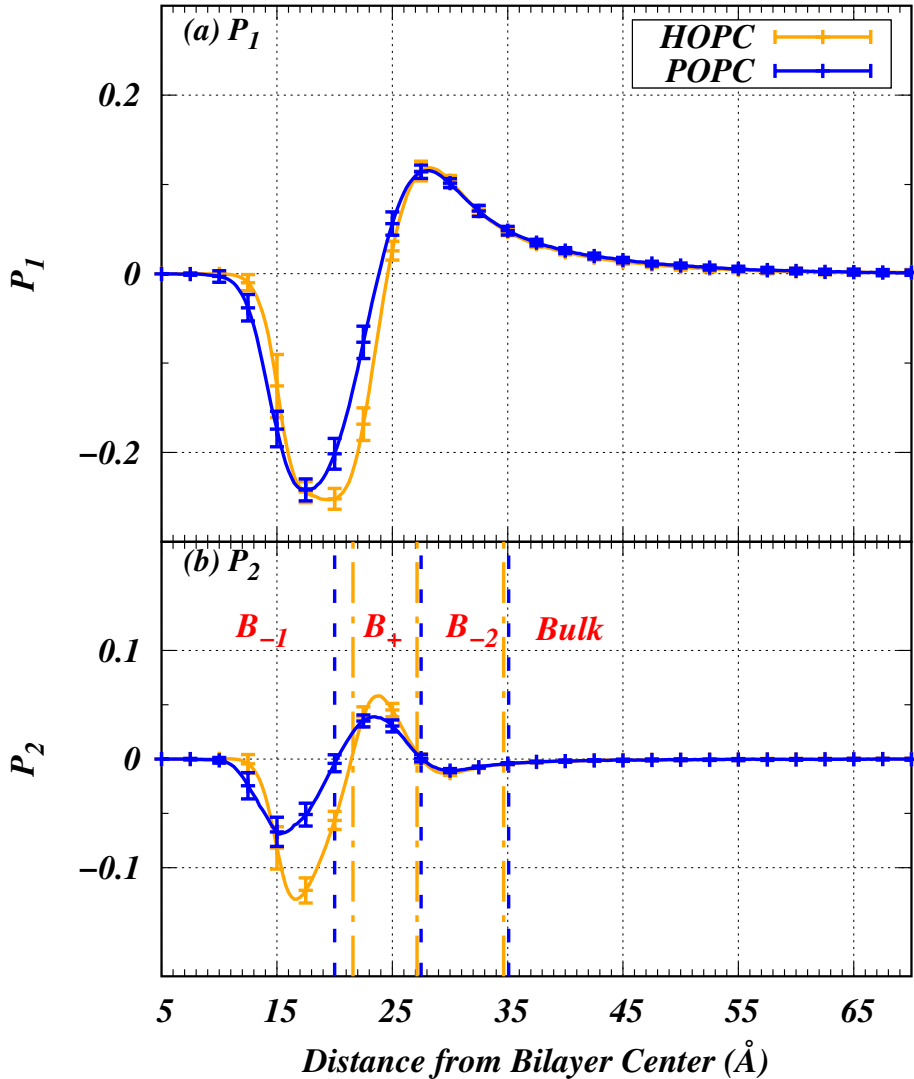


Figure 2.7: The first and second order parameters,  $P_1$  and  $P_2$ , of water O-H bonds. Each parameter is calculated by first dividing the simulation box into 2000 slices, and then averaging the data separately in each slice. The box is symmetrized around the bilayer center, and thus only half the box is shown. Standard deviations are calculated by dividing the trajectory into over 5ns blocks. The dashed vertical lines in the  $P_2$  plot are demarcations for the different spatial regions,  $B_{-1}$ ,  $B_+$ ,  $B_{-2}$ , and  $B_{\text{bulk}}$ , as discussed in the associated text.  $P_1$  is the average of the first legendre polynomial of the cosine of the angle between the bilayer normal and the O-H bond vector of each water molecule per box slice.  $P_2$  is the average of the second legendre polynomial. Looking to  $P_1$ , both systems exhibit similar magnitudes of ordering.  $P_2$  shows a more complicated distribution, with larger magnitudes of ordering in all regions in the HOPC system.

274 for the remainder of the paper. For the purpose of counting the number of waters in the  
275 surface, we truncated the box at this boundary, to a length of 35 ångströms. Numbers of  
276 perturbed waters per lipid for each system can be seen in table 2.1 line 8.

277 We also use these order parameters to compute the quadrupolar splitting of water as  
278 measured in NMR experiments. It is essentially a weighted average of the second order  
279 parameter, similar to the one derived by Kruczek *et al.*:<sup>16</sup>

$$\Delta\nu = \frac{3}{4}\chi \frac{1}{N_w} \sum_{z_i=0}^{z_0} n_w(z_i) P_2(z_i), \quad (2.5)$$

280 where the number of perturbed waters in the system is  $N_w$ ,  $n_w$  is the number of waters in  
281 each slice of the box, and  $P_2(z_i)$  is the value of the second order parameter in the  $i^{\text{th}}$  slice.

282 We take the quadrupolar splitting constant of water  $\chi = 220\text{KHz}$  from Åman *et al.*<sup>55</sup> The  
283 summation over slices is carried out from the bilayer center ( $z = 0$ ) to the end of the box.

284 We report that the quadrupolar splitting of water in the POPC system is 194.99 Hz, and  
285 that in the HOPC system is 1756.08 Hz (also shown in table 2.1, line 9). These values  
286 reflect a similar difference to what we observed in our earlier comparative study of ether-  
287 and ester-linked lipid bilayers in pure water.<sup>16</sup>

288 Next we compute the lateral diffusion coefficient of water. To gain detailed insight, we  
289 compute it separately for four different regions along the bilayer normal. We define these  
290 regions using the  $P_2(z)$  profile:  $B_{-1}$  is the region closest to the bilayer center where  $P_2(z)$  is  
291 negative;  $B_+$  is the region where  $P_2(z)$  is positive;  $B_{-2}$  is the region beyond the  $B_+$  boundary  
292 where  $P_2(z)$  is negative; and the remaining portion beyond  $B_{-2}$  we refer to as bulk. These  
293 regions are also labeled in figure 2.7. The diffusion coefficients for waters in these regions  
294 are included in table 2.2. They are calculated using Einstein's relationship, and a protocol  
295 detailed in our previous study.<sup>16</sup> Taking note of the overall pattern, the lateral diffusion  
296 decreases progressively as one moves deeper into the bilayer. Additionally, in the innermost  
297 regions  $B_{-1}$  and  $B_+$  water diffuses more slowly in HOPC compared to POPC. This result is

	$B_{-1}$ ( $\text{nm}^2/\text{s}$ )	$B_+$ ( $\text{nm}^2/\text{s}$ )	$B_{-2}$ ( $\text{nm}^2/\text{s}$ )	Bulk ( $\text{nm}^2/\text{s}$ )
HOPC	$0.85 \pm 0.59$	$1.783 \pm 0.94$	$16.1 \pm 5.24$	$26.67 \pm 0.65$
POPC	$1.075 \pm 0.62$	$3.078 \pm 0.74$	$16.27 \pm 5.19$	$27.30 \pm 0.66$

Table 2.2: Diffusion coefficients of water measured in  $\text{nm}^2/\text{s}$  in different regions along the bilayer normal (see figure 2.7 and related text for the definitions of the different spatial regions. The two innermost-bilayer regions  $B_{-1}$  and  $B_+$  in HOPC contain waters that have a greatly lowered diffusion coefficient. In the regions  $B_{-2}$  and bulk, the bilayer composition does not seem to change the diffusion behavior. These values were calculated using the method outlined in previous work by our lab<sup>16</sup> The various regions are illustrated on figure 2.7.

298 similar to what we observed previously<sup>16</sup> in simulations without salt.

299 To characterize the orientational dynamics of waters, we compute autocorrelations of the  
300 O-H bonds,

$$C^{O-H}(t) = \left\langle \vec{v}_{O-H}(0) \cdot \vec{v}_{O-H}(t) \right\rangle. \quad (2.6)$$

301 We calculate expectation values separately for all the 2 Å slices along the bilayer normal by  
302 tracking individual water molecules for 500ps, and also averaging over all waters in the slice.  
303 We also weight each water by the fraction of duration it spends in each slice. This is done in  
304 5 ns chunks, and then averaged over the trajectories. We then model these autocorrelations  
305 as a sum of three exponential terms,

$$C^{O-H}(t) = A_1 e^{-t/\tau_1} + A_2 e^{-t/\tau_2} + (1 - A_1 - A_2) e^{-t/\tau_3}, \quad (2.7)$$

306 where  $A_i$  are positive, and  $\tau_i$  are correlation times. Fitting is carried out using the Marquardt-  
307 Levenberg least-squares fitting method. The correlation times are plotted in figure 2.8.

308 We find that  $\tau_1$  shows a profile similar to what we observed for ether- and ester-lipids  
309 simulated in pure water.<sup>16</sup> Additionally, we find that the correlation times  $\tau_1$  and  $\tau_2$  in the  
310 HOPC bilayer are all longer than in POPC. The maximum correlation times of 1838 ps in  
311 HOPC and 1019 ps in POPC are characteristic of rotationally immobile waters inside the

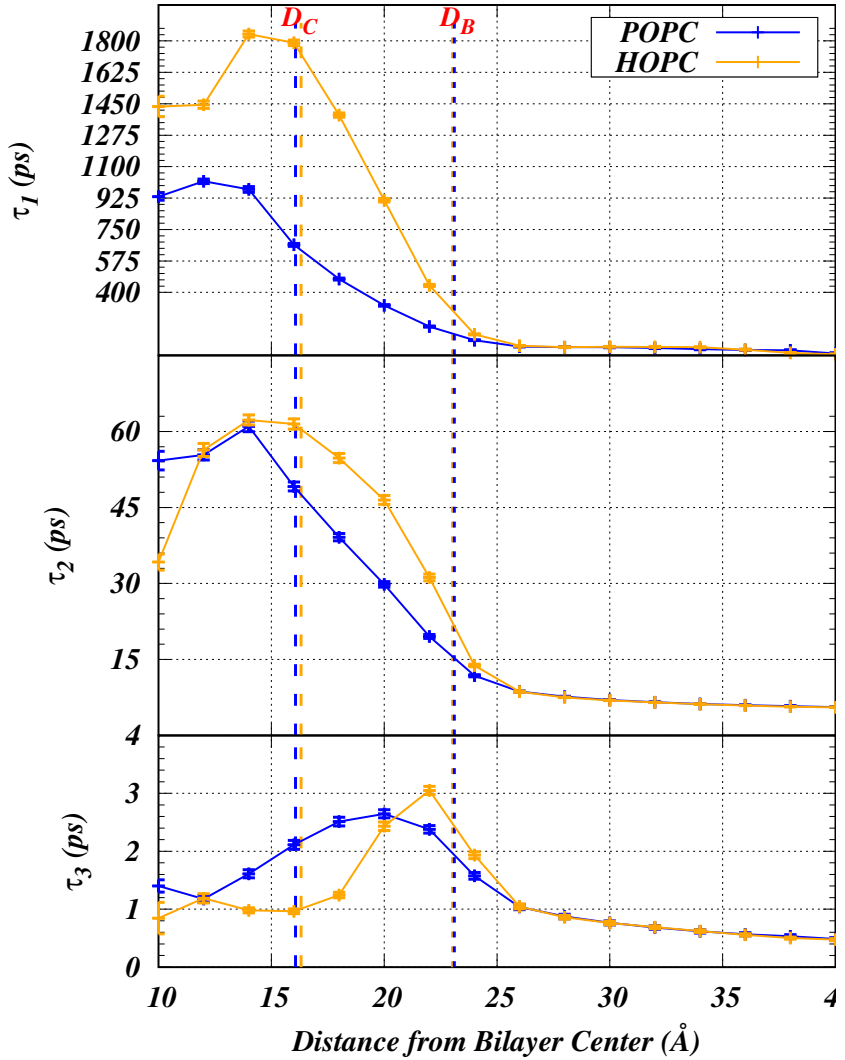


Figure 2.8: Orientational autocorrelation times of O-H bonds in water, as determined by modeling their autocorrelations using three-exponential fits. No values are shown for at distances less than 12 Å from the bilayer center, as there are no waters in this region. The dashed vertical lines indicate chain boundaries  $D_c$  and bilayer thickness  $D_b/2$ , colored to indicate the lipid system.

<sup>312</sup> bilayer surface and also of crystallographically-resolved waters in protein-protein interfaces.<sup>56</sup>

<sup>313</sup> Note that  $\tau_3$ , which is of the order of picoseconds, is close to the sampling time of our  
<sup>314</sup> trajectories. Thus, we regard it simply as a fitting parameter.

<sup>315</sup> Overall, we find that the headgroup water in HOPC is significantly more organized and  
<sup>316</sup> also diffuses more slowly as compared to the headgroup water in POPC. This is similar to  
<sup>317</sup> what we had observed<sup>16</sup> when we compared another diether lipid bilayer against its chemically  
<sup>318</sup> analogous diester-lipid bilayer, but in the absence of NaCl. This leads us to conclude that  
<sup>319</sup> in ether-linked lipid bilayers water forms a rigid and immobile layer within the headgroup  
<sup>320</sup> region of the bilayer, and exposure to a moderate concentration of salt does not disrupt this  
<sup>321</sup> layer.

### <sup>322</sup> 2.2.4 Bilayer electrostatics

<sup>323</sup> The dipole potential of a bilayer is the potential difference between the inside of the  
<sup>324</sup> bilayer and bulk water. In our previous comparative study of ether- and ester-linked bilayers  
<sup>325</sup> in pure water<sup>16</sup> we had found that the dipole potential of the ether-linked lipid bilayer was  
<sup>326</sup>  $56 \pm 5$  mV smaller than that of the ester-linked lipid bilayer, and this finding was consistent  
<sup>327</sup> with experiment.<sup>13</sup> We also know that membrane association with salt can modify its dipole  
<sup>328</sup> potential, with increases of around 200mV from that of a bilayer without salt reported  
<sup>329</sup> previously.<sup>19,57,58</sup>

<sup>330</sup> Figure 2.9 compares the electrostatic potential in HOPC and POPC as a function of  
<sup>331</sup> distance along the bilayer normal. These are calculated from an integration of the one  
<sup>332</sup> dimensional Poisson's equation,

$$\phi(z) = -\frac{1}{\epsilon_0} \int_0^z \int_0^{z'} \rho(z) dz dz' + C_1 z + C_2, \quad (2.8)$$

<sup>333</sup> where  $\rho(z)$  is the charge density along the bilayer normal, and  $\epsilon_0$  is the vacuum permittivity.

<sup>334</sup> Note that we integrate this equation using two boundary conditions — the electric field in

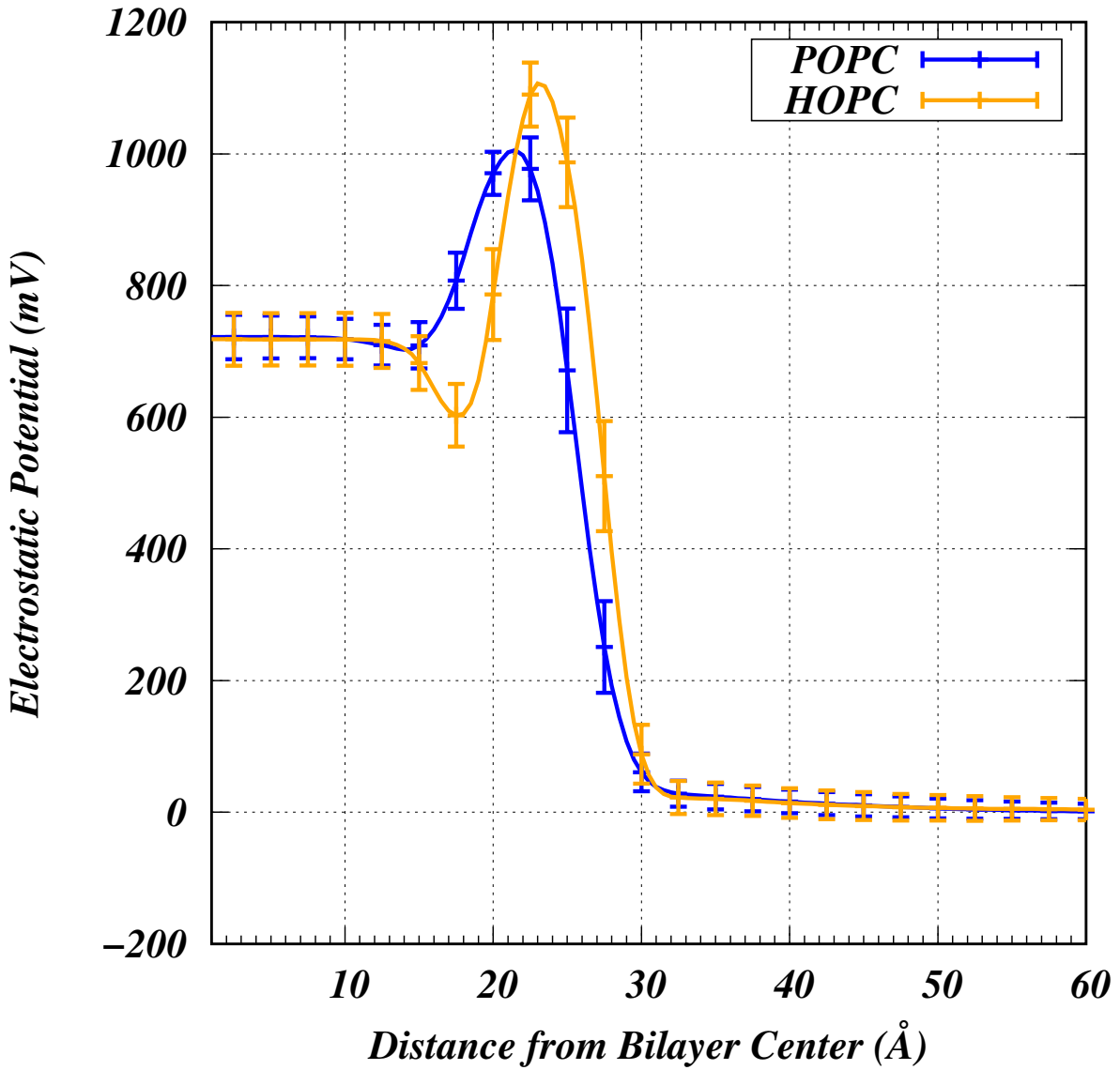


Figure 2.9: Comparison of electrostatic potentials between the HOPC and POPC systems. These distributions are calculated by integrating the charge density of our systems twice, assuming the potential goes to zero at the box edge and that the electric field of bulk solvent is zero. Looking to the region from the bilayer center to around 10 Å, one can see the bilayer dipole potential. We see very similar values for this in both systems. We also see a large peak in the HOPC system, and a large trough that is not present in POPC. The larger peak at the bilayer surface may provide a barrier to solvent and dissolved ions, and the trough may be a trap that causes the buildup of solvent in the bilayer headgroup region.

335 bulk water is zero, yielding  $C_2 = 0$ , and the potential at the simulation box boundary is also  
336 zero, which makes  $C_1 = 0$ .

337 The first observation we make is that the dipole potentials of both HOPC and POPC are  
338 similar; a behavior distinct from that observed in simulations in pure water. Nevertheless,  
339 the overall electrostatic potential profiles are similar to those observed in pure water. Firstly,  
340 a characteristic peak near the phosphate region still exists, and this peak is higher for the  
341 diether lipid bilayer. This could potentially serve as a higher permeation barrier in the  
342 diether-linked lipid system. This interpretation is consistent with our observation above  
343 that there are fewer membrane-associated ions in HOPC compared to POPC. Secondly, the  
344 diether-linked lipid system had a trough next to the peak, which is absent in the diester-  
345 linked lipid bilayer, and may serve as a trap for solvent molecules. In fact, the spatial location  
346 of the trough corresponds to the high water density region in the HOPC bilayer.

### 347 2.2.5 Salt distribution at the bilayer-solvent interface

348 The behavior of salt near bilayer surfaces is often modeled using Gouy-Chapman theory;  
349 a mean-field approximation that has its roots in Poisson-Boltzman theory.<sup>3,59</sup> This theory  
350 also forms the basis for electrophoretic mobility studies.<sup>59,60</sup> In this theory, water is modeled  
351 as a dielectric continuum in which ion particles behave as an uncorrelated gas. This means  
352 that the number density distribution of ions in the dielectric continuum only depends on the  
353 temperature and the electrostatic potential applied to the system.

354 So far, due to limitations from system size and ionic force field parameters, we have  
355 refrained from comparing or validating our simulations at the atomistic level against this  
356 theory. Here, we show convergence between these atomistic simulations and the Poisson-  
357 Boltzman theory.

358 Within Poisson-Boltzmann theory, the number density of ions near the bilayer surface is  
359 described as

$$\rho(z) = \rho_0 \exp(-\bar{z}e\beta\psi(z)), \quad (2.9)$$

where  $\rho_0$  is the ion density in the bulk,  $\bar{z}$  is the valency of the ion,  $\beta = (k_b T)^{-1}$ ,  $e$  is the charge on an electron, and  $\psi(z)$  is the electrostatic potential. We define the interfaces as the *hydration boundaries* (see subsection 2.2.3 ‘Water structure and dynamics’). The lengths of the solvent occupied regions,  $D$ , in each of the two systems are listed in table 2.3. We set the center of this solvent occupied region as  $z = 0$ , which then implies that the interfaces are essentially at  $z = \pm D/2$  nm, as illustrated in figure 2.10. We model  $\psi(z)$  as a sum of two Debye-Huckle potentials,<sup>3</sup> each a reflection of the other around the center of the solvent occupied region:

$$\psi_1(z) = \psi_s \exp\left(-K(z + \frac{D}{2})\right) \quad (2.10)$$

$$\psi_2(z) = \psi_s \exp\left(K(z - \frac{D}{2})\right) \quad (2.11)$$

$$\psi(z) = \psi_1(z) + \psi_2(z) - (\psi_1(0) + \psi_2(0)) \quad (2.12)$$

<sup>360</sup> Here  $\psi_s = \sigma/\epsilon_0 \epsilon K$  is the electrostatic potential at the bilayer surface, where  $\sigma$  is the surface  
<sup>361</sup> charge density of the bilayer leaflet.<sup>3</sup>  $K$  is the inverse Debye length,

$$K = \sqrt{\sum_i \rho_{0,i} \bar{z}_i^2 \frac{e^2}{\epsilon_0 \epsilon k_b T}}, \quad (2.13)$$

<sup>362</sup> where the sum of  $\rho_{0,i}$ ’s is over all the included ions in our system. Note that in Equ. 2.12

	$K(\text{nm}^{-1})$	$D$ nm	$\rho_0$ ( $\text{nm}^{-3}$ )	$\sigma$ ( $e \text{ nm}^{-2}$ )
POPC	$0.98 \pm 0.021$	$13.167 \pm 0.0071$	$0.043 \pm 0.0018$	0.13
HOPC	$1.09 \pm 0.037$	$13.752 \pm 0.0068$	$0.060 \pm 0.0041$	0.128

Table 2.3: Parameters in Gouy-Chapman theory.  $K$  was calculated using equation 2.13. This was done using the value for  $\rho_0$  for each system, found by taking the average number density of  $\text{Cl}^-$  ions within the solvent-occupied region of the box. The charge density  $\sigma$  was calculated by integrating the charge of the ions from the bilayer center to the surface at 35 Å from the bilayer center for each system, shown to be the *hydration boundary* of both bilayers.  $D$  gives the length of the solvent-occupied region of each simulation box.

<sup>363</sup> we subtract out the value of the potential at the center of the solvent occupied region from  
<sup>364</sup>  $\psi(z)$ . Note also that the form of  $\psi_s$  is valid only for small surface potentials, generally  
<sup>365</sup> those smaller than 20 millivolts.<sup>3</sup> Our systems have a relatively small surface charges (See  
<sup>366</sup> table 2.3), which will result in small surface potentials (See table 2.3). The surface charges  
<sup>367</sup> are calculated by integrating charge densities of ions contained behind the surface. We chose  
<sup>368</sup> to do this because all other parts of the simulated system are uncharged, and the surface is  
<sup>369</sup> entirely charged by the adsorbed ions.

<sup>370</sup> Figure 2.11 compares the potential and ion distribution obtained from theory against  
<sup>371</sup> those estimated directly from simulations.

<sup>372</sup> We note a very close match between the two. Additionally, we find that HOPC shows  
<sup>373</sup> a slightly larger  $K$  than POPC, indicating a  $\sim$ 10% shorter screening length for the system.  
<sup>374</sup> This means that a bilayer of HOPC is better shielded from environmental electric fields. The  
<sup>375</sup> shorter screening length in the HOPC is also reflective of the smaller number of ions that  
<sup>376</sup> adsorb onto the surface of the bilayer, as this directly results in a larger number density in  
<sup>377</sup> bulk solvent due to the fixed number of ions in our system.

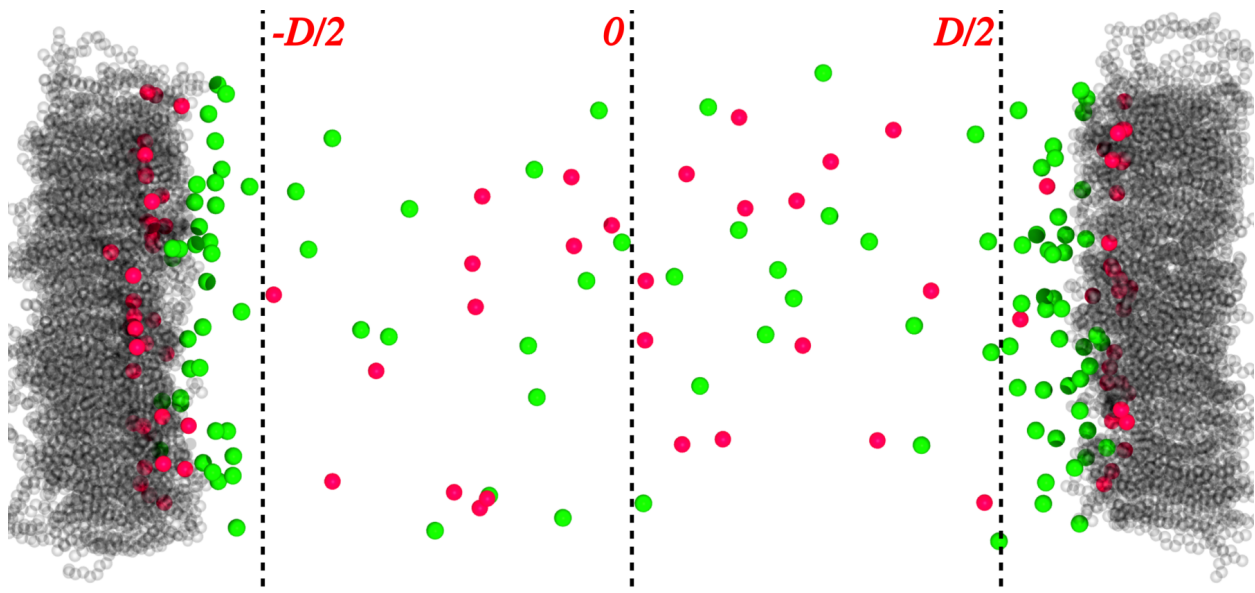


Figure 2.10: Illustration of bulk ion distribution, with surfaces used in Gouy-Chapman theory calculations. For the purpose of illustration, solvent has been hidden from this image.  $\text{Cl}^-$  ions have been colored in green, and  $\text{Na}^+$  ions are shown in red. Surfaces set at the *hydration boundary* of each bilayer leaflet are shown with dotted lines. The center of the solvent occupied region of the box is set at zero.

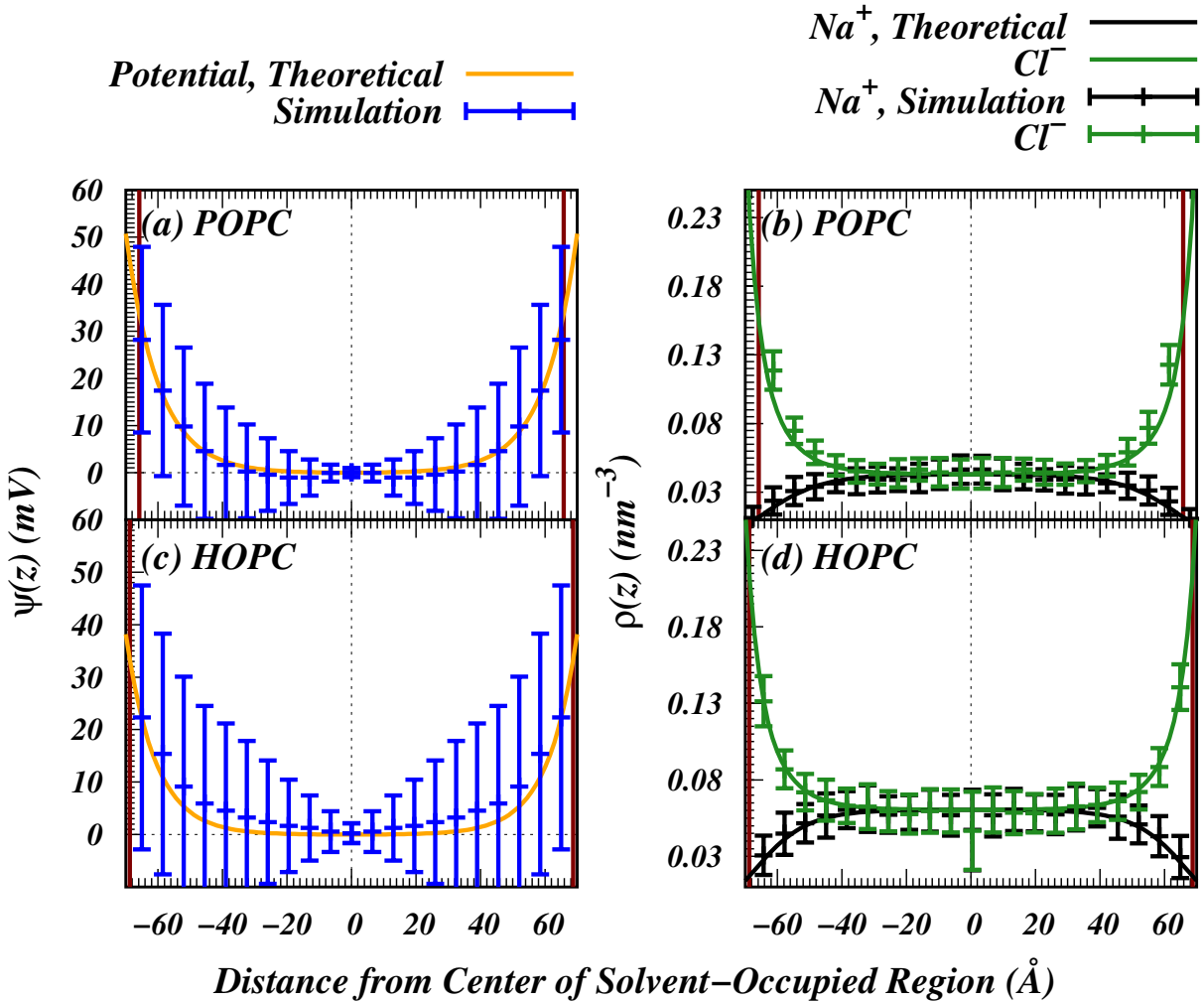


Figure 2.11: Comparison of Gouy-Chapman theory predictions and simulation results. Theoretical distributions are given by the solid lines, and data from our simulations are shown as points with error bars. (a) and (c) show the electrostatic potentials of each system. For clarity, we show error-bars for the simulation results for every 13th point. The Debye-Huckle potentials shown follow the form given in equation 2.12. (b) and (d) show the number density distribution of ions in each system. Error-bars for the simulation results are shown for every 30th point. Note that both systems are translated to center around the solvent-occupied region of the box, giving an interspace region of  $\sim 13$  nm in each system. Parameters used in Gouy-Chapman theory are in table 2.3

378

## CHAPTER 3

379

## CONCLUSIONS

380 Phospholipids are an important part of all living things, acting as the major constituent  
381 of cellular plasma membranes. The great variety of phospholipid species allows organisms  
382 another parameter to fine-tune the behavior and structure of their membranes in order to  
383 adapt to a wide range of different environments.<sup>1</sup> Ether-linked lipids are a major distin-  
384 guishing feature of archael membranes, have been suggested in the past to be an adaptation  
385 to archaeal membranes to tune flexibility and permeability of their membranes to extreme  
386 environments.<sup>9,61</sup>

387 In our work, we have found that ether-linked lipid bilayers show a distinct peak in solvent  
388 density that is not disrupted by the inclusion of a moderate concentration of salt. This region  
389 shows significantly reduced lateral diffusion, and longer autocorrelation times than the same  
390 region in an analogous ester-linked lipid bilayer. Furthermore, we find that the characteristic  
391 lower dipole potential of an ether-linked bilayer reported in previous work<sup>16</sup> is increased to  
392 match that of the ester-linked bilayer in the presence of salt. We also find that, with our new  
393 protocol for determining the interface boundary of the lipid bilayer, our simulations model  
394 ion distributions and electrostatic potentials from Gouy-Chapman theory well. The shorter  
395 screening length in the ether-linked system suggests better shielding from electric fields far  
396 from the bilayer compared to the ester-linked system. This is a result of the ether-linked  
397 lipid bilayer's lower affinity for ions than the ester-linked analog.

## BIBLIOGRAPHY

- [1] G. Van Meer, D. R. Voelker, G. W. Feigenson, Membrane lipids: where they are and how they behave, *Nature reviews Molecular cell biology* 9 (2) (2008) 112.
- [2] S. A. Pandit, H. L. Scott, Simulations and models of lipid bilayers, in: *Soft Matter: Lipid Bilayers and Red Blood Cells*, Vol. 4, Wiley Online Library, 2008, Ch. 1, pp. 1–82.
- [3] J. N. Israelachvili, *Intermolecular and surface forces*, Academic press, 2011.
- [4] M. Ashrafuzzaman, J. A. Tuszynski, *Membrane biophysics*, Springer Science & Business Media, 2012.
- [5] W. Humphrey, A. Dalke, K. Schulten, VMD – Visual Molecular Dynamics, *Journal of Molecular Graphics* 14 (1996) 33–38.
- [6] J. B. Reece, L. A. Urry, M. L. Cain, S. A. Wasserman, P. V. Minorsky, R. B. Jackson, et al., *Campbell biology*, no. s 1309, Pearson Boston, 2014.
- [7] Y.-M. Zhang, C. O. Rock, Membrane lipid homeostasis in bacteria, *Nature Reviews Microbiology* 6 (3) (2008) 222.
- [8] S. Sehgal, M. Kates, N. Gibbons, Lipids of halobacterium cutirubrum, *Canadian journal of biochemistry and physiology* 40 (1) (1962) 69–81.
- [9] Y. Koga, From promiscuity to the lipid divide: on the evolution of distinct membranes in archaea and bacteria, *Journal of molecular evolution* 78 (3-4) (2014) 234–242.

- 417 [10] M. Kates, Membrane lipids of archaea, in: The biochemistry of archaea (archaeabacteria),  
418 Vol. 26, Elsevier, 1993, Ch. 9, pp. 261–295.
- 419 [11] S. D. Guler, D. D. Ghosh, J. Pan, J. C. Mathai, M. L. Zeidel, J. F. Nagle, S. Tristram-  
420 Nagle, Effects of ether vs. ester linkage on lipid bilayer structure and water permeability,  
421 Chemistry and physics of lipids 160 (1) (2009) 33–44.
- 422 [12] M. Jansen, A. Blume, A comparative study of diffusive and osmotic water permeation  
423 across bilayers composed of phospholipids with different head groups and fatty acyl  
424 chains, Biophysical journal 68 (3) (1995) 997–1008.
- 425 [13] K. Gawrisch, D. Ruston, J. Zimmerberg, V. Parsegian, R. Rand, N. Fuller, Membrane  
426 dipole potentials, hydration forces, and the ordering of water at membrane surfaces,  
427 Biophysical journal 61 (5) (1992) 1213–1223.
- 428 [14] N. S. Haas, P. Sripada, G. G. Shipley, Effect of chain-linkage on the structure of  
429 phosphatidyl choline bilayers. hydration studies of 1-hexadecyl 2-palmitoyl-sn-glycero-  
430 3-phosphocholine, Biophysical journal 57 (1) (1990) 117–124.
- 431 [15] J. C. Fogarty, M. Arjunwadkar, S. A. Pandit, J. Pan, Atomically detailed lipid bilayer  
432 models for the interpretation of small angle neutron and x-ray scattering data, Biochimica  
433 et Biophysica Acta (BBA)-Biomembranes 1848 (2) (2015) 662–672.
- 434 [16] J. Kruczak, M. Saunders, M. Khosla, Y. Tu, S. A. Pandit, Molecular dynamics simu-  
435 lations of ether-and ester-linked phospholipids, Biochimica et Biophysica Acta (BBA)-  
436 Biomembranes 1859 (12) (2017) 2297–2307.
- 437 [17] A. N. Leonard, R. W. Pastor, J. B. Klauda, Parameterization of the charmm all-atom  
438 force field for ether lipids and model linear ethers, The Journal of Physical Chemistry  
439 B (2018).

- 440 [18] J. Kruczak, S.-W. Chiu, S. Varma, E. Jakobsson, S. A. Pandit, Interactions of mono-  
441 valent and divalent cations at palmitoyl-oleoyl-phosphatidylcholine interface, *Langmuir*  
442 35 (32) (2019) 10522–10532.
- 443 [19] J. Kruczak, S.-W. Chiu, E. Jakobsson, S. A. Pandit, Effects of lithium and other monova-  
444 lent ions on palmitoyl oleoyl phosphatidylcholine bilayer, *Langmuir* 33 (4) (2017) 1105–  
445 1115, pMID: 28076953. arXiv:<http://dx.doi.org/10.1021/acs.langmuir.6b04166>,  
446 doi:[10.1021/acs.langmuir.6b04166](https://doi.org/10.1021/acs.langmuir.6b04166).  
447 URL <http://dx.doi.org/10.1021/acs.langmuir.6b04166>
- 448 [20] N. Duro, M. Gjika, A. Siddiqui, H. L. Scott, S. Varma, Popc bilayers supported on  
449 nanoporous substrates: specific effects of silica-type surface hydroxylation and charge  
450 density, *Langmuir* 32 (26) (2016) 6766–6774.
- 451 [21] G. Pabst, A. Hodzic, J. Štrancar, S. Danner, M. Rappolt, P. Laggner, Rigidification of  
452 neutral lipid bilayers in the presence of salts, *Biophysical journal* 93 (8) (2007) 2688–  
453 2696.
- 454 [22] J. N. Sachs, H. Nanda, H. I. Petracche, T. B. Woolf, Changes in phosphatidylcholine  
455 headgroup tilt and water order induced by monovalent salts: molecular dynamics sim-  
456 ulations, *Biophysical journal* 86 (6) (2004) 3772–3782.
- 457 [23] H. I. Petracche, S. Tristram-Nagle, D. Harries, N. Kučerka, J. F. Nagle, V. A. Parsegian,  
458 Swelling of phospholipids by monovalent salt, *Journal of lipid research* 47 (2) (2006)  
459 302–309.
- 460 [24] R. O. Dror, R. M. Dirks, J. Grossman, H. Xu, D. E. Shaw, Biomolecular simulation: a  
461 computational microscope for molecular biology, *Annual review of biophysics* 41 (2012)  
462 429–452.

- 463 [25] D. P. Tieleman, S.-J. Marrink, H. J. Berendsen, A computer perspective of membranes:  
464 molecular dynamics studies of lipid bilayer systems, *Biochimica et Biophysica Acta*  
465 (BBA)-Reviews on Biomembranes 1331 (3) (1997) 235–270.
- 466 [26] D. Frenkel, B. Smit, Understanding molecular simulation: from algorithms to applica-  
467 tions, Vol. 1, Elsevier, 2001.
- 468 [27] H. Li, J. Chowdhary, L. Huang, X. He, A. D. MacKerell Jr, B. Roux, Drude polarizable  
469 force field for molecular dynamics simulations of saturated and unsaturated zwitterionic  
470 lipids, *Journal of chemical theory and computation* 13 (9) (2017) 4535–4552.
- 471 [28] J. W. Ponder, C. Wu, P. Ren, V. S. Pande, J. D. Chodera, M. J. Schnieders, I. Haque,  
472 D. L. Mobley, D. S. Lambrecht, R. A. DiStasio Jr, et al., Current status of the amoeba  
473 polarizable force field, *The journal of physical chemistry B* 114 (8) (2010) 2549–2564.
- 474 [29] O. Berger, O. Edholm, F. Jähnig, Molecular dynamics simulations of a fluid bilayer  
475 of dipalmitoylphosphatidylcholine at full hydration, constant pressure, and constant  
476 temperature, *Biophysical journal* 72 (5) (1997) 2002–2013.
- 477 [30] S. Chiu, M. Clark, E. Jakobsson, S. Subramaniam, H. L. Scott, Optimization of hydro-  
478 carbon chain interaction parameters: application to the simulation of fluid phase lipid  
479 bilayers, *The Journal of Physical Chemistry B* 103 (30) (1999) 6323–6327.
- 480 [31] S. Chiu, S. Vasudevan, E. Jakobsson, R. J. Mashl, H. L. Scott, Structure of sphin-  
481 gomyelin bilayers: a simulation study, *Biophysical journal* 85 (6) (2003) 3624–3635.
- 482 [32] S.-W. Chiu, S. A. Pandit, H. Scott, E. Jakobsson, An improved united atom force field  
483 for simulation of mixed lipid bilayers, *The Journal of Physical Chemistry B* 113 (9)  
484 (2009) 2748–2763.
- 485 [33] J. F. Nagle, S. Tristram-Nagle, Structure of lipid bilayers, *Biochimica et Biophysica*  
486 *Acta* (BBA)-Reviews on Biomembranes 1469 (3) (2000) 159–195.

- 487 [34] M. L. Berkowitz, D. L. Bostick, S. Pandit, Aqueous solutions next to phospholipid  
488 membrane surfaces: insights from simulations, *Chemical reviews* 106 (4) (2006) 1527–  
489 1539.
- 490 [35] F. Jähnig, What is the surface tension of a lipid bilayer membrane?, *Biophysical journal*  
491 71 (3) (1996) 1348–1349.
- 492 [36] K. Raghavan, M. R. Reddy, M. L. Berkowitz, A molecular dynamics study of the struc-  
493 ture and dynamics of water between dilauroylphosphatidylethanolamine bilayers, *Lang-  
494 muir* 8 (1) (1992) 233–240.
- 495 [37] S. J. Marrink, M. Berkowitz, H. J. Berendsen, Molecular dynamics simulation of a  
496 membrane/water interface: the ordering of water and its relation to the hydration force,  
497 *Langmuir* 9 (11) (1993) 3122–3131.
- 498 [38] E. Egberts, S.-J. Marrink, H. J. Berendsen, Molecular dynamics simulation of a phos-  
499 pholipid membrane, *European biophysics journal* 22 (6) (1994) 423–436.
- 500 [39] S.-W. Chiu, M. Clark, V. Balaji, S. Subramaniam, H. L. Scott, E. Jakobsson, Incor-  
501 poration of surface tension into molecular dynamics simulation of an interface: a fluid  
502 phase lipid bilayer membrane, *Biophysical journal* 69 (4) (1995) 1230–1245.
- 503 [40] M. J. Abraham, T. Murtola, R. Schulz, S. Páll, J. C. Smith, B. Hess, E. Lindahl,  
504 Gromacs: High performance molecular simulations through multi-level parallelism from  
505 laptops to supercomputers, *SoftwareX* 1 (2015) 19–25.
- 506 [41] S. Pall, M. J. Abraham, C. Kutzner, B. Hess, E. Lindahl, Tackling exascale software  
507 challenges in molecular dynamics simulations with gromacs, in: International Confer-  
508 ence on Exascale Applications and Software, Springer, 2014, pp. 3–27.
- 509 [42] D. V. D. Spoel, E. Lindahl, B. Hess, G. Groenhof, A. Mark, H. Berendsen, Gromacs:  
510 fast, flexible, free, *J. Comput. Chem.* 26 (2005) 1701.

- 511 [43] E. Lindahl, B. Hess, D. Van Der Spoel, Gromacs 3.0: a package for molecular simulation  
512 and trajectory analysis, Molecular modeling annual 7 (8) (2001) 306–317.
- 513 [44] H. J. Berendsen, D. van der Spoel, R. van Drunen, Gromacs: a message-passing par-  
514 allel molecular dynamics implementation, Computer Physics Communications 91 (1-3)  
515 (1995) 43–56.
- 516 [45] H. Berendsen, J. Grigera, T. Straatsma, The missing term in effective pair potentials,  
517 Journal of Physical Chemistry 91 (24) (1987) 6269–6271.
- 518 [46] I. S. Joung, T. E. Cheatham III, Determination of alkali and halide monovalent ion pa-  
519 rameters for use in explicitly solvated biomolecular simulations, The journal of physical  
520 chemistry B 112 (30) (2008) 9020–9041.
- 521 [47] S. Nosé, M. Klein, Constant pressure molecular dynamics for molecular systems, Molec-  
522 ular Physics 50 (5) (1983) 1055–1076.
- 523 [48] M. Parrinello, A. Rahman, Polymorphic transitions in single crystals: A new molecular  
524 dynamics method, Journal of Applied physics 52 (12) (1981) 7182–7190.
- 525 [49] B. Hess, H. Bekker, H. J. C. Berendsen, J. G. E. M. Fraaije, Lincs: A linear  
526 constraint solver for molecular simulations, Journal of Computational Chemistry  
527 18 (12) (1997) 1463–1472. doi:10.1002/(SICI)1096-987X(199709)18:12<1463::  
528 AID-JCC4>3.0.CO;2-H.  
529 URL [http://dx.doi.org/10.1002/\(SICI\)1096-987X\(199709\)18:12<1463::  
530 AID-JCC4>3.0.CO;2-H](http://dx.doi.org/10.1002/(SICI)1096-987X(199709)18:12<1463::AID-JCC4>3.0.CO;2-H)
- 531 [50] U. Essmann, L. Perera, M. L. Berkowitz, T. Darden, H. Lee, L. G. Pedersen, A smooth  
532 particle mesh ewald method, The Journal of chemical physics 103 (19) (1995) 8577–8593.

- 533 [51] H. I. Petrache, S. E. Feller, J. F. Nagle, Determination of component volumes of lipid  
534 bilayers from simulations., *Biophysical Journal* 72 (5) (1997) 2237–2242.  
535 URL <http://www.ncbi.nlm.nih.gov/pmc/articles/PMC1184418/>
- 536 [52] E. Egberts, H. Berendsen, Molecular dynamics simulation of a smectic liquid crystal  
537 with atomic detail, *The Journal of chemical physics* 89 (6) (1988) 3718–3732.
- 538 [53] J.-P. Douliez, A. Leonard, E. J. Dufourc, Restatement of order parameters in biomem-  
539 branes: calculation of cc bond order parameters from cd quadrupolar splittings., *Bio-*  
540 *physical journal* 68 (5) (1995) 1727.
- 541 [54] S. Varma, S. B. Rempe, Structural transitions in ion coordination driven by changes  
542 in competition for ligand binding, *Journal of the American Chemical Society* 130 (46)  
543 (2008) 15405–15419.
- 544 [55] K. Åman, E. Lindahl, O. Edholm, P. Håkansson, P.-O. Westlund, Structure and dynam-  
545 ics of interfacial water in an  $l\alpha$  phase lipid bilayer from molecular dynamics simulations,  
546 *Biophysical journal* 84 (1) (2003) 102–115.
- 547 [56] P. Dutta, M. Botlani, S. Varma, Water dynamics at protein–protein interfaces: Molecu-  
548 lar dynamics study of virus–host receptor complexes, *The Journal of Physical Chemistry*  
549 B 118 (51) (2014) 14795–14807.
- 550 [57] M. L. Berkowitz, D. L. Bostick, S. Pandit, Aqueous solutions next to phospholipid  
551 membrane surfaces: insights from simulations, *Chemical reviews* 106 (4) (2006) 1527–  
552 1539.
- 553 [58] A. Cordomi, O. Edholm, J. J. Perez, Effect of ions on a dipalmitoyl phosphatidylcholine  
554 bilayer. a molecular dynamics simulation study, *The Journal of Physical Chemistry B*  
555 112 (5) (2008) 1397–1408.

- 556 [59] P. Wiersema, A. Loeb, J. T. G. Overbeek, Calculation of the electrophoretic mobility  
557 of a spherical colloid particle, *Journal of Colloid and Interface Science* 22 (1) (1966)  
558 78–99.
- 559 [60] R. W. O'Brien, L. R. White, Electrophoretic mobility of a spherical colloidal particle,  
560 *Journal of the Chemical Society, Faraday Transactions 2: Molecular and Chemical  
561 Physics* 74 (1978) 1607–1626.
- 562 [61] D. L. Valentine, Adaptations to energy stress dictate the ecology and evolution of the  
563 archaea, *Nat Rev Micro* 5 (4) (2007) 316–323.  
564 URL <http://dx.doi.org/10.1038/nrmicro1619>